Available online at www.sciencedirect.com
SCIENCE DIRECT®
PERGAMON
Electrochimica Acta 48 (2003) 2933–2942
ELECTROCHIMICA Acta
www.elsevier.com/locate/electacta

# Surface combinatorial studies of IR properties of nanostructured Ru film electrodes using CO as probe molecule

Hui Gong, Shi-Gang Sun *,[1], Jun-Tao Li, You-Jiang Chen, Sheng-Pei Chen

*State Key Laboratory for Physical Chemistry of Solid Surfaces, Department of Chemistry, Institute of Physical Chemistry, Xiamen University, Xiamen 361005, China*

Received 12 December 2002; received in revised form 16 April 2003; accepted 17 April 2003

**Abstract**

An individually addressable array of Pt microelectrodes was designed and prepared. Ru film of different nanostructures was prepared electrochemically on platinum microelectrodes of the array under cyclic voltammetric conditions. The electrochemical behavior and surface structure of the Ru film were investigated, respectively, using cyclic voltammetry and scanning tunneling microscopy. In combining the individually addressable array with an in situ microscope FTIR reflection spectroscopy (MFTIRS), surface combinatorial studies of IR properties of different nanostructured Ru films have been conveniently carried out. In situ microscope FTIR spectral library of CO adsorbed on different nanostructured Ru films and at different electrode potentials was acquired rapidly. Particular IR properties of nanostructured Ru film were revealed. IR absorption of both bridge-bonded CO ($CO_B$, around 1800 $cm^{-1}$) and linearly bonded CO ($CO_L$, near 2000 $cm^{-1}$) was significantly enhanced, and an enhancement factor of IR absorption has been determined to be varied between 11.8 and 15.5 along with the variation of nanostructure of Ru film on the array. Following consecutive increase in thickness of Ru film and in size of Ru islands that form the film, $CO_B$ species yielded always a broad band appearing in anti-absorption direction, while $CO_L$ species produced an IR band that was transformed from a bipolar shape to monopolar shape of anti-absorption direction. Together with the shift of IR band center, the large increase in IR bandwidth and in Stark tuning rate, the particular IR properties were illustrated as a change from Fano-like asymmetric spectral characteristics to abnormal IR features, and attributed to the consecutive variation of nanostructure of Ru film on the individually addressable array.


*Keywords:* Surface combinatorial study; Nanostructured Ru film; Abnormal infrared effects; In situ microscope FTIRS; Individually addressable array

## 1. Introduction

Nanoparticles and nanostructured film of platinum group metals and alloys are used widely as electrocatalysts for direct fuel cells [1–4]. We have revealed in previous papers [5–9] that nanostructured film of platinum group metals (Pt, Pd, Rh and Ru) and alloys (PtRu, PtPd) supported on glassy carbon exhibits abnormal infrared effects (AIREs). The AIREs consist in that, in comparison with CO or other molecules ($SCN^-$, $CN^-$, etc.) adsorbed on a bulk metal electrode, the same molecule adsorbed on electrode of nanostructured film yielded three typical abnormal IR features, which are: (1) the inversion of the direction of IR bands, i.e., the direction of IR bands of adsorbates is inverted from absorption to anti-absorption; (2) the significant enhancement of IR absorption of adsorbates; (3) the increase in the full-width at half-maximum (FWHM) of IR bands. Christensen et al. [10] have observed also an inversion of CO band direction in the case of methanol

* Corresponding author. Tel.: +86-59-22180181; fax: +86-59-22183047.
*E-mail address:* sgsun@xmu.edu.cn (S.-G. Sun).
[1] ISE member.

0013-4686/03/$ - see front matter © 2003 Elsevier Ltd. All rights reserved.
doi:10.1016/S0013-4686(03)00358-X

oxidation on carbon electrode covered by platinum nanoparticles. Similar specific IR properties of Ir [11] and Os [12] thin films supported on glassy carbon, Pt ultrathin film supported on silicon [13] and platinized platinum film [14] were also reported recently. The AIREs as well as surface-enhanced Raman scattering (SERS) [15], surface-enhanced infrared absorption (SEIRA) [16,17], surface-enhanced second harmonic generation (SESHG) [18] and surface-enhanced sum frequency generation (SESFG) [19] are all closely related with nanostructured materials. Going deep insight into the AIREs is of significant interest not only in studying the particular properties of nanostructure of two-dimensional material, but also in developing fundamental of related fields such as electrocatalysis, IR spectroscopy, material science, etc. In order to reveal the origin of the AIREs, a systematic study on the relationship between film nanostructure and IR optical properties may be most helpful. It is therefore convenient to develop a combinatorial method of surface electrochemistry for such studies. The combinatorial method of surface electrochemistry will allow acquiring an in situ IR spectral library of multi-electrodes at defined conditions, facilitating the comparison and the analysis of IR data of different nanostructure of film material.

The idea of development of a combinatorial method of surface electrochemistry is from the combinatorial chemistry, i.e., in its essence based on the principle of parallelism [20]. It is strategy to allow scientists not only quickly synthesizing large sets of samples with limited number of starting material, but also analyzing all of them in a short time [21]. It is therefore considerably beneficial in screening out the objects with target properties. The combinatorial chemistry has attracted much more attentions in the field of the discovery of inorganic material with superior properties [22–24]. Exploiting and developing high-throughput, optical screening method is at one center of interests in the research of combinatorial chemistry [25]. The method of combinatorial chemistry has also been developed in applications of heterogeneous catalysis and electrocatalysis towards direct methanol fuel cells [26].

We have established recently a new technique named as electrochemical in situ microscope FTIR spectroscopy (MFTIRS) [27]. It has advantages of a spatial resolution in IR investigation. In this paper, different nanostructured Ru films were prepared by electrodeposition on an individually addressable array of Pt microelectrodes. Combinatorial studies of surface electrochemistry were carried out by combining the in situ MFTIRS with the individually addressable array. The main goal of this study consists in revealing the intrinsic relationship of IR properties and nanostructure of Ru film.

## 2. Experimental

### 2.1. Preparation of an individually addressable array of Pt microelectrodes

The individually addressable array of Pt microelectrodes was fabricated by passing nine Pt wires of 200 μm in diameter through a Teflon template. The nine platinum microelectrodes (PtME) were arranged in a $3 \times 3$ array. The coordinate of each PtME is denoted as $ME_{ij}$, ME means microelectrode, the subscripts $i$ and $j$ indicate the $i$th row and $j$th column on the array. The center-to-center distance between neighbouring microelectrodes was fixed at 1.0 mm. It was confirmed that the coupling effects between the PtME could be neglected at such separation. A homemade switch box was designed to allow selectively connecting any PtME, or any arbitrary group of PtME or all PtME to potentiostat. The structures of the individually addressable array Pt microelectrodes are schematically illustrated in Fig. 1a.

### 2.2. Apparatus and principle

The configurations of in situ MFTIRS have been described in our earlier reports [27,28]. An IR microscope (IR-plan advantage, Spectra Tech, Inc.) equipped with a liquid-$N_2$ cooled MCT-A detector is attached to a Nexus 870 FTIR spectrometer (Nicolet). The structure of Microscope IR Cell is illustrated in Fig. 1b. A platinum wire and a Pd wire charged in saturation with hydrogen (Pd|H) were served as auxiliary and reference electrodes, respectively. The potentials presented in the paper are referring to the Pd|H electrode scale. In all IR experiment, non-polarized beam was employed to study IR optical features of nanostructured Ru films. The angle of incident IR beam is about 32°. The spot of microscope IR beam, without using any optical aperture, shed on substrate is about 330 μm in diameter. The result spectra of electrochemical in situ MFTIRS was calculated according to $\Delta R/R = (R(E_S) - R(E_R))/E_R$, where $R(E_R)$ is the IR single-beam spectrum of reflectance collected at reference potential $E_R$ and

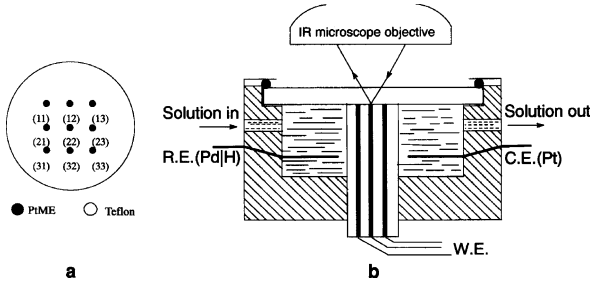


Fig. 1. Schematic diagram of individually addressable array of Pt microelectrodes: (a) the configuration of the array of Pt microelectrodes; (b) schematic structure of electrochemical in situ MFTIRS cell.

$R(E_S)$ the IR single-beam spectra of reflectance collected at sample potential $E_S$. In this study, $E_R$ was chosen as 1.00 V at which CO was completely oxidized and $E_S$ was varied between 0.00 and 0.50 V where $CO_{ad}$ on Ru film electrode is stable or partially oxidized. The experimental procedure was arranged in such a way that the $R(E_S)$ at all $E_S$ was collected firstly and then the electrode potential was stepped to $E_R$ to collect $R(E_R)$. The collection of $R(E_S)$ and $R(E_R)$ were carried out sequentially on the array of PtME. According to the definition of $\Delta R/R$, the direction of IR band of CO adsorbed on a bulk Ru electrode will present negative-going monopolar bands in resulting spectra, as observed by different groups [29–32]. In order to obtain satisfied signal-to-noise ratio (S/N), 100 interferograms were collected and co-added into each single-beam spectrum. The spectral resolution of the spectra was 8 $cm^{-1}$.

### 2.3. Other conditions

Prior to electrodeposition of Ru onto PtME that was served as substrate, the individually addressable array of PtME was polished mechanically using sand paper, alumina powder of size 5, 1, 0.3 and 0.05 μm. After cleaning in an ultrasonic bath, the array of PtME was subjected to voltammetric cycling between 0.00 and 1.58 V in 0.1 $mol\,l^{-1}$ $H_2SO_4$ at a scan rate of 0.10 V $s^{-1}$, until a reproducible cyclic voltammogram (CV) of Pt electrode was obtained. Then the array was transferred into a Ru plating solution containing 0.1 $mol\,l^{-1}$ $H_2SO_4$ and $2.0 \times 10^{-3}$ M $Ru^{3+}$ ions. Method of cyclic voltammetry was used to deposit electrochemically Ru film on each PtME of the array. The lower and upper limits of potential scan in cyclic voltammetry applied for Ru deposition were −0.23 and 0.37 V, respectively, and the sweep rate was 0.05 V $s^{-1}$. The thickness as well as the nanostructure of Ru films were controlled by varying the number of potential cycles ($n$) in the deposition. During the procedure of electrodeposition of Ru, $N_2$ gas of high purity was bubbled into the solution to drive away $H_2$ that was produced at the surface of Ru film in low potential region. The nanostructured Ru film electrodeposited on PtME of the array is denoted subsequently as Ru($n$)/PtME, where $n$ is the number of cycles of potential scan that applied in electrodeposition of Ru film. After the preparation, the individually addressable array of Ru($n$)/PtME was transferred to another cell containing 0.1 M $H_2SO_4$ solution, and subjected to a pre-treatment of cyclic potential scan between 0.00 and 0.78 V at a scan rate of 0.10 V $s^{-1}$ to reduce possible surface Ru oxide and to clean the surface. The stable cyclic voltammograms were then recorded. For the sake of briefness, the allocation of Ru($n$)/PtME on the array was listed in Table 1. In the FTIR experiment, adsorption of CO was carried out in CO saturation 0.1 $mol\,l^{-1}$ $H_2SO_4$ solution through a potential cycling between 0.00 and 0.25 V at a scan rate of 0.10 V $s^{-1}$ until saturation adsorption of CO was achieved. Electrolytes used in this study were prepared with super-pure sulphuric acid and Millipore water provided from a Milli-Q Labo apparatus (Millipore Ltd., Japan). All experiments were carried out at room temperature around 20 °C.

The investigation of surface structures of the nine Ru($n$)/PtME on the array was carried out on a P4-18-SPM scanning tunneling microscope (NT-MDT, Russia).

## 3. Results and discussion

### 3.1. Studies of cyclic voltammetry

Fig. 2 shows the cyclic voltammograms of Ru($n$)/PtME (solid curves) on the array in 0.1 $mol\,l^{-1}$ $H_2SO_4$ solution at a scan rate 0.10 V $s^{-1}$. In order to facilitate discussion, a cyclic voltammogram of a PtME (dot curve) is also displayed in the graph. It can be seen that all Ru($n$)/PtME exhibit similar CV characteristics that differ from those of the PtME. In all curves of Ru($n$)/PtME, a pair of anodic and cathodic peaks in low potential region between 0.00 and 0.25 V can be observed. They are ascribed to adsorption/desorption of hydrogen adatoms. When the potential in the anodic sweep increases, an oxidation peak between 0.25 and 0.65 V starts to appear, which is due to formation of adsorbed OH species ($OH_{ad}$) on Ru film surface. When continuously increasing the potential, the oxidation current appeared in the CV may be ascribed to the generation of surface oxides. The $OH_{ad}$ species and oxides formed in the anodic sweep are reduced in the cathodic sweep, which gives rise to a very broad peak ranging from 0.75 to 0.12 V.

Since all PtME on the array have an identical geometric area of $3.14 \times 10^{-4}$ $cm^{-2}$, the value of current density ($j$) of Ru($n$)/PtME in cyclic voltammo-

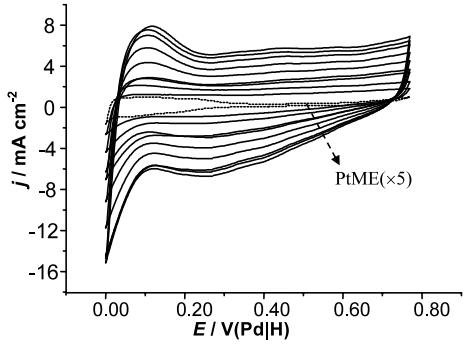


Fig. 2. Comparison of stable cyclic voltammograms of a PtME (dotted curve) and Ru($n$)/PtME (solid curves) on the array in 0.1 $mol\,l^{-1}$ $H_2SO_4$ solution, sweep rate 0.10 V $s^{-1}$, the current of the PtME is enlarged by 5 times.

Table 1
The allocation of Ru($n$)/PtME on the array

| $ME_{ij}$ | $ME_{11}$ | $ME_{12}$ | $ME_{13}$ | $ME_{21}$ | $ME_{22}$ | $ME_{23}$ | $ME_{31}$ | $ME_{32}$ | $ME_{33}$ |
|---|---|---|---|---|---|---|---|---|---|
| $n$ | 50 | 90 | 130 | 170 | 210 | 250 | 290 | 330 | 370 |

grams is directly proportional to the real surface area. It can be seen that the value of $j$ is increased with the increase of $n$. This result indicates that the real surface area of Ru($n$)/PtME could be continuously augmented under such electrodeposition conditions. The surface relative roughness of Ru($n$)/PtME ($R_r$) is calculated by comparing the electric charge integrated from CV curves of hydrogen adsorption–desorption potential region measured from Ru($n$)/PtME with that of a PtME, i.e.,

$$R_r = \frac{Q_H^n}{Q_H^{n=0}} \quad (1)$$

where $Q_H^n$ is the charge of Ru($n$)/PtME and $Q_H^{n=0}$ is the charge of PtME that is measured to be 0.56 mC cm$^{-2}$ from Fig. 2. The values of $R_r$ are listed in Table 2.

### 3.2. STM studies of surface structure of Ru($n$)/PtME on the array

The surface structure of Ru($n$)/PtME on the array was studied ex situ by using scanning tunneling microscope. The nine STM images of the same scan size, 1.35 μm × 1.35 μm, are displayed in Fig. 3. It can be seen that the island-shaped Ru crystallites were formed on the PtME substrate in cyclic voltammetric deposition. This result is different from that obtained on Ru film electrodeposited on glassy carbon. In that case, Ru crystallites of hexagonal shape arranged in a layer structure were observed [7]. It is evident that such difference in film structure can be ascribed to the substrate material used in experiment. It is well known that GC is an amorphous material and has quite different chemical structure from Ru metal. However, Pt and Ru have analogous properties for they all belonging to platinum metal group. The different properties of GC and Pt lead to different mechanisms of electro-crystallization of Ru, and thus result in different surface structure of Ru film.

It can be clearly seen that continuous electrodeposition leads to consecutive change in surface structure of Ru($n$)/PtME on the array. With the help of an home-made simple software, the dimension of Ru islands in STM images can be conveniently measured. It was found that the average size of Ru islands ($\bar{d}$) on $ME_{11}$ is about 79.7 nm. Mechanical polishing scratches can also be observed on $ME_{11}$ and $ME_{12}$, because of rather thin film overlaid on the PtME substrate. With $n$ increases, $\bar{d}$ grows gradually. $\bar{d}$ is measured at 169.2 nm on $ME_{21}$ ($n = 170$) and 196.4 nm on $ME_{33}$ ($n = 370$). They are about 2.1 and 2.5 times larger in comparison with that measured on $ME_{11}$, respectively.

With the help of statistic facilities provided by the STM software package, the average thickness ($\bar{l}$) of nanostructured Ru film of each Ru($n$)/PtME on the array can be calculated by the following equation:

$$\bar{l} = \frac{1}{N^2} \sum_{i=1}^{n} \sum_{j=1}^{n} |Z_{(i,j)}| \quad (2)$$

where $|Z_{(i,j)}|$ is the height of the pixel $(i,j)$ in an STM image. In this study, $N$ equals 512, and so in total $512^2 = 262\,144$ points were involved in the calculation. Another parameter $R_q$, i.e., the root mean square of the absolute value of the surface departures form the mean plane, is calculated by

$$R_q = \sqrt{\frac{1}{n^2} \sum_{i=1}^{n} \sum_{j=1}^{n} (Z_{(i,j)} - \bar{l})^2} \quad (3)$$

It is evident that $R_q$ may be considered as the error in $\bar{l}$ measurement. $R_q$ also effectively represents the surface roughness of the Ru film. Fig. 4 displays the histogram of $\bar{l}$ and $R_q$ of each Ru($n$)/PtME on the array. In comparison, $\bar{l}$ and $R_q$ are, respectively, measured to be 15.8 and 4.8 nm on a PtME. After electrodepositing Ru on the surface of PtME, both values of $\bar{l}$ and $R_q$ are increased. It can be seen that large quantity of electrodeposited Ru leads to produce a rougher surface, e.g., the values of $\bar{l}$ and $R_q$ from $ME_{11}$ to $ME_{33}$ increase with $n$. Table 3 lists the structural parameters of Ru($n$)/PtME on the array measured from STM images.

Table 2
CV characterization of Ru($n$)/PtME on the array

| | $ME_{ij}$ | | | | | | | | |
|---|---|---|---|---|---|---|---|---|---|
| | $ME_{11}$ | $ME_{12}$ | $ME_{13}$ | $ME_{21}$ | $ME_{22}$ | $ME_{23}$ | $ME_{31}$ | $ME_{32}$ | $ME_{33}$ |
| $Q_H^n$ (mC cm$^{-2}$) | 1.42 | 2.67 | 3.24 | 4.13 | 5.27 | 6.99 | 7.75 | 8.86 | 9.92 |
| $R_r$ | 2.5 | 4.7 | 5.7 | 7.3 | 9.4 | 12.4 | 13.8 | 15.8 | 17.7 |

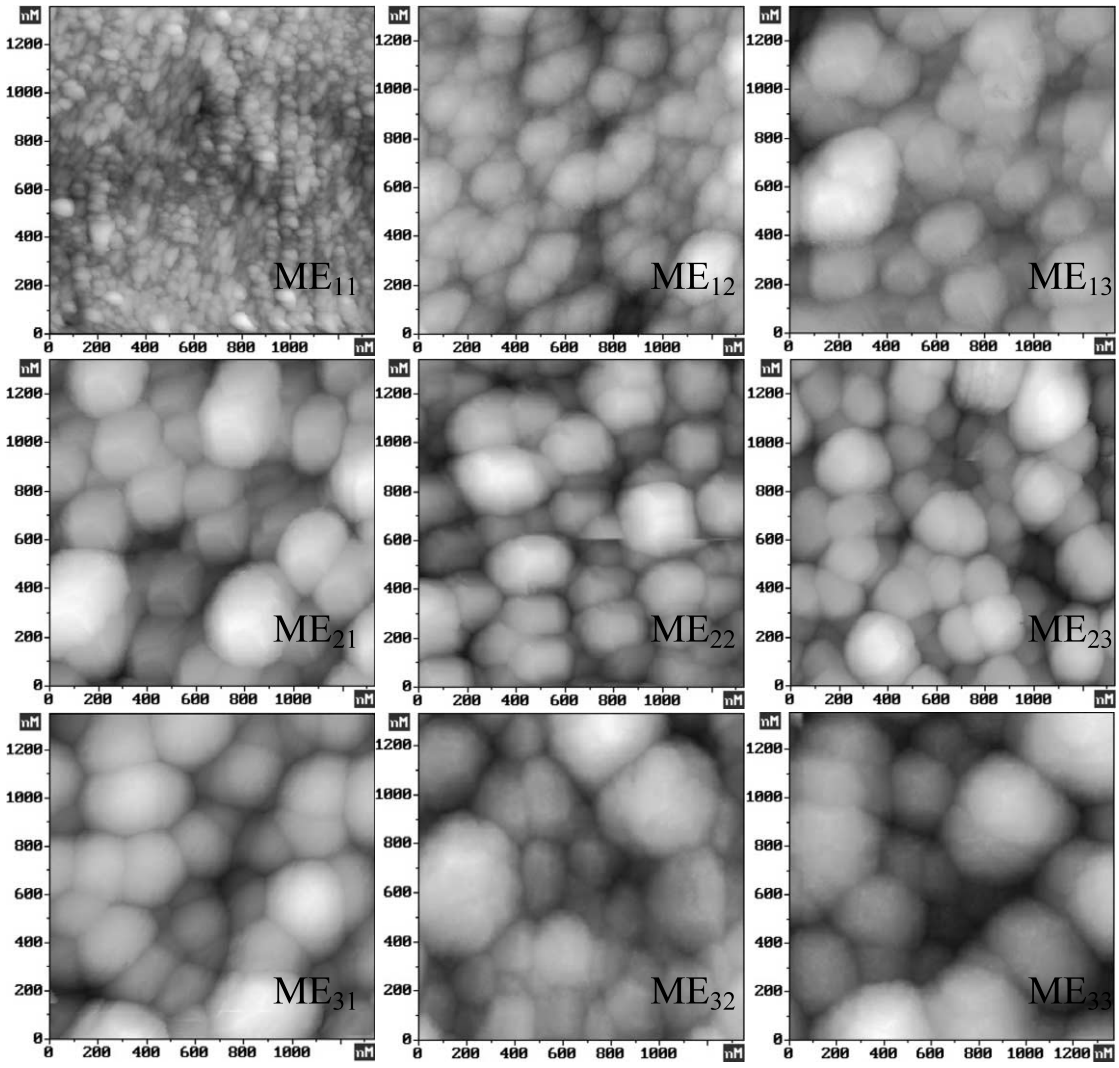


Fig. 3. STM images of Ru($n$)/PtME on the array. Scan size: 1.35 μm × 1.35 μm, $I_t = 0.401$ nA, $V_b = 0.15$ V.

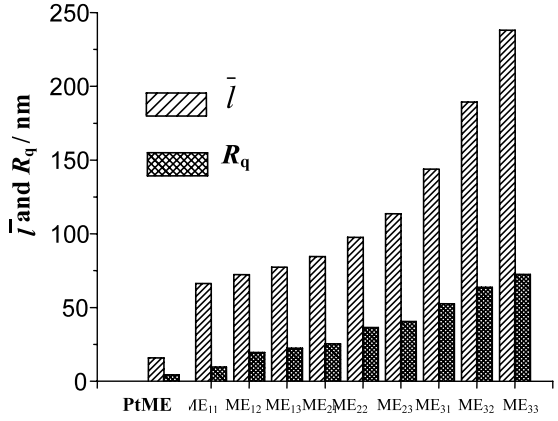


Fig. 4. Variation of $\bar{l}$ and $R_q$ measured from STM images of Ru($n$)/PtME on the array, and a PtME subjected to mechanically and electrochemically polishing.

### 3.3. In situ MFTIRS studies of CO adsorbed on Ru($n$)/PtME on the array

The data listed in Table 3 and the STM images illustrated in Fig. 3 indicate that nanostructure of Ru thin film is varied consecutively on the array. In this section, the adsorption of CO was employed as a molecule probe reaction, and surface combinatorial studies were conducted by combining in situ MFTIRS with individually addressable array of nanostructured Ru film electrodes. In situ MFTIR spectra of all Ru($n$)/PtME on the array at different electrode potentials were recorded under the same conditions. In order to present clearly different IR properties of different nanostructure of Ru film on the array, we discuss at first two particular cases of $ME_{33}$ and $ME_{13}$.

#### 3.3.1. IR features of CO adsorbed on Ru(370)/PtME

In situ MFTIR spectra of CO adsorbed on $E_{33}$ ($n$ = 370) in CO saturation 0.1 M $H_2SO_4$ solutions recorded

Table 3
List of structural parameters of Ru($n$)/PtME measured from STM images

| | $ME_{ij}$ | | | | | | | | |
|---|---|---|---|---|---|---|---|---|---|
| | $ME_{11}$ | $ME_{12}$ | $ME_{13}$ | $ME_{21}$ | $ME_{22}$ | $ME_{23}$ | $ME_{31}$ | $ME_{32}$ | $ME_{33}$ |
| $\bar{l}$ (nm) | 66.3 | 72.2 | 77.4 | 84.6 | 97.5 | 113.4 | 143.7 | 189.4 | 238.1 |
| $R_q$ | 7.7 | 14.9 | 16.6 | 19.9 | 27.8 | 32.0 | 40.0 | 46.4 | 57.2 |
| $\bar{d}$ (nm) | 79.7 | 143.3 | 161.8 | 169.2 | 172.7 | 177.0 | 180.2 | 187.7 | 196.4 |

at different electrode potentials are shown in Fig. 5a. A negative-going and strong band around 1650 $cm^{-1}$ is attributed to IR absorption of water ($\delta_{HOH}$ mode), which may be originated from the complete oxidation of adsorbed CO at $E_R$, i.e.,

$$CO_{ad} + H_2O \rightarrow CO_2 + 2H^+ + 2e^- \quad (4)$$

The consumption of $H_2O$ at $E_R$ makes that IR absorption of $H_2O$ is stronger in the single-beam spectrum $R(E_S)$ than that in the single-beam spectrum $R(E_R)$; as a consequence a negative-going band appears in the potential-difference spectrum. It is worthy to note that the potential-dependent reorientation of $H_2O$ molecule on electrode surface [33] may also make appearing a $\delta_{HOH}$ band at around 1650 $cm^{-1}$ in the potential-difference spectrum. We observe a positive-going band near 1200 $cm^{-1}$ that does not shift with electrode potential. In consideration of solution used in study, this band can be attributed to surface adsorption of anion $SO_4^{2-}$ species at $E_R$. In order to facilitate the discussion of IR features of adsorbed CO ($CO_{ad}$) on Ru(370)/PtME, a spectrum of CO adsorbed on the substrate PtME electrode is displayed in Fig. 5b for comparison. Since $CO_{ad}$ is completely oxidized at $E_R$, the IR absorption of $CO_{ad}$ will yield negative-going bands. This is true for IR absorption of linear-bonded CO ($CO_L$) on PtME, which appears a negative-going band around 2065 $cm^{-1}$ at $E_S = 0.00$ V. However, the IR absorption of $CO_{ad}$ on Ru(370)/PtME yields positive-going bands, i.e., a $CO_L$ band near 1970 $cm^{-1}$ and a broad band around 1750 $cm^{-1}$. The positive-going direction of the $CO_{ad}$ bands indicates IR anti-absorption of CO adsorbed on this nanostructured Ru film. It is worthwhile mentioning that the inversion of direction of adsorbate IR bands on nanostructured film material is one of the important IR features of AIREs [6,34].

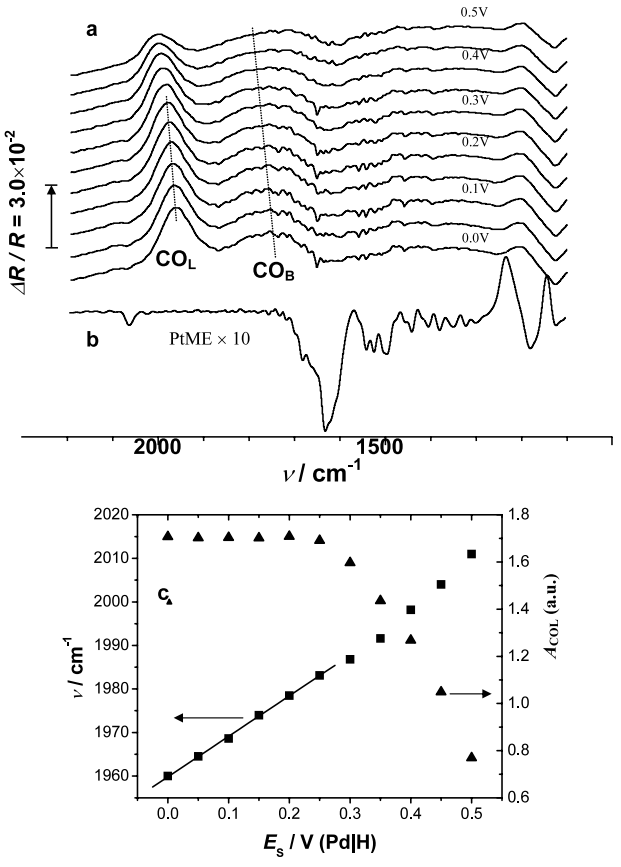


Fig. 5. The comparison of in situ IR spectra of CO adsorbed on (a) Ru(370)/PtME ($E_S$ is indicated in figure, $E_R = 1.00$ V); (b) PtME ($E_S = 0.00$ V, $E_R = 1.00$ V) in 0.1 mol $l^{-1}$ $H_2SO_4$ solution (CO saturated); (c) potential dependencies of band center and integrated intensity of the $CO_L$ band on Ru(370)/PtME.

We can also observe other two typical IR features of AIREs on the Ru(370)/PtME in Fig. 5a: (1) the intensity of the $CO_L$ band is much larger in spectra recorded on Ru(370)/PtME than that in the spectrum recorded on PtME. In comparison with the IR band intensity of $CO_{ad}$ on a bulk Ru reported by Lin et al. [30], the IR absorption of $CO_{ad}$ on Ru(370)/PtME is remarkably enhanced. The fact that the appearance of $CO_B$ band in spectra recorded on Ru($n$)/PtME confirms also the enhancement of IR absorption; (2) the FWHM of the $CO_L$ band measured from spectra recorded on Ru(370)/PtME is 90 $cm^{-1}$, while that measured from spectrum recorded on PtME is only 20 $cm^{-1}$. This value of FWHM on Ru(370)/PtME seems surprisingly large. It is even about 37 $cm^{-1}$ larger than the FWHM value (53 $cm^{-1}$) of $CO_L$ band in spectra recorded on electrode of nanometer thin Ru film supported on GC substrate that exhibits typical AIREs [7].

Fig. 5c displays variations of $CO_L$ band center ($\nu_{CO_L}$) and integrated intensity of the $CO_L$ band ($A_{CO_L}$) versus $E_S$. The $A_{CO_L}$ keeps almost constant in the potential region from 0.00 to 0.25 V, while it decreases gradually as $E_S$ is increased above 0.25 V. It can also be observed

from Fig. 5a that the intensity of the $CO_B$ band is decreased in accordance with the decrease of $A_{CO_L}$. It is evident that the decrease in intensity of the $CO_{ad}$ bands corresponds to oxidation of $CO_{ad}$ species. The result suggests that the onset potential of $CO_{ad}$ oxidation on Ru(370)/PtME is about 0.25 V, which is lower than the onset oxidation potential of CO adsorbed on a bulk Ru (0.4 V/RHE in 0.1 M $HClO_4$, i.e., about 0.36 V (Pd|H) in 0.1 M $H_2SO_4$) [30] or on a nanometer thin Ru film electrodeposited on GC (0.10 V (SCE), i.e., about 0.37 V (Pd|H)) [7], indicating a higher activity of the nanostructured Ru film on PtME for CO oxidation. It is known that the PtRu alloy is a best CO-tolerant catalyst in direct methanol fuel cells [35]. The higher electrocatalytic activity for CO oxidation of Ru(370)/PtME than that of nanometer thin Ru film on GC is certainly originated from an synergy effect of interaction between Ru thin film and PtME substrate [36]. It can be observed from Fig. 5c that the $\nu_{CO_L}$ varies with $E_S$ as a straight line bellow 0.25 V, while deviates from the straight line when $E_S$ is exceeded 0.25 V. It is known that the variation of $\nu_{CO_L}$ with $E_S$ yields two straight lines for CO adsorbed on a bulk Ru [30] or on a nanometer thin Ru film substrated on GC [7], and the slope of the straight line laid in high potential region is larger than that at low potential region. It is evident that the deviation of variation of $\nu_{CO_L}$ with $E_S$ at potentials above 0.25 V is due to oxidation of $CO_{ad}$. The Stark tuning rate ($d\nu_{CO_L}/dE$) is therefore measured from the straight line to be 93 $cm^{-1}$ $V^{-1}$, which is much larger than the value (34 $cm^{-1}$ $V^{-1}$) measured for CO adsorbed on nanometer thin Ru film (86 nm of film thickness) substrated on GC [7] and the value (52 $cm^{-1}$ $V^{-1}$) obtained in case of CO adsorbed on a bulk Ru electrode [30] with $E_S$ varying in similar potential range.

The above results demonstrated clearly that the $ME_{33}$ on the array, i.e., the Ru(370)/PtME electrode, exhibits abnormal IR effects for CO adsorption, which consists in the inversion of the direction of $CO_{ad}$ bands, the significant enhancement of IR absorption of $CO_{ad}$, and the large increase both in the FWHM of $CO_{ad}$ bands and in the Stark tuning rate.

### 3.3.2. IR features of CO adsorbed on Ru(130)/PtME

Fig. 6a displays in situ MFTIR spectra of CO adsorbed on $ME_{13}$ ($n = 130$) for $E_S$ varying from 0.00 to 0.50 V in CO saturation 0.1 M $H_2SO_4$ solutions. The IR absorption of $CO_L$ appears unexpectedly as a bipolar band that consists of a positive peak at around 2035 $cm^{-1}$ (anti-absorption) and a negative peak near 1980 $cm^{-1}$ (absorption). Nevertheless, $CO_B$ band still appears as a positive-going band. As stated previously, the $CO_{ad}$ has been oxidized completely at $E_R$, the bipolar IR feature of the $CO_L$ band comes uniquely from IR absorption of $CO_L$ at $E_S$. In order to confirm this point, a series of $R(E_R)$ was recorded sequentially at different

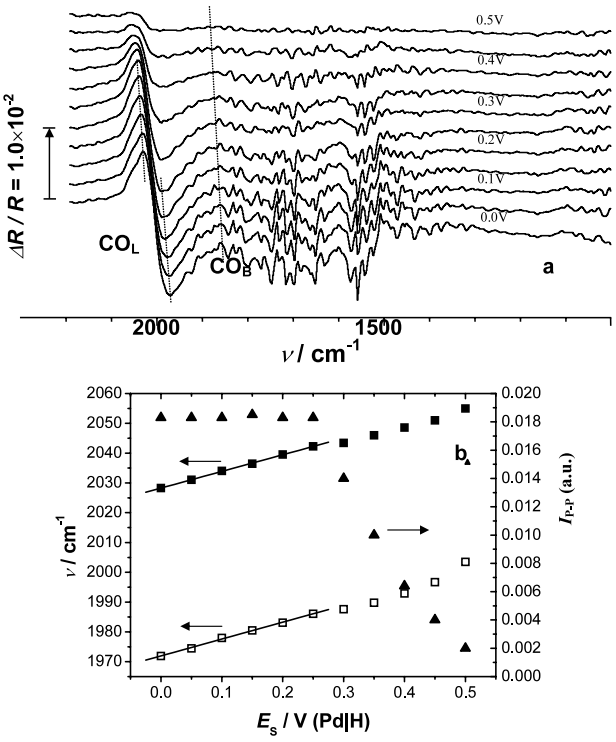


Fig. 6. (a) In situ FTIR spectra of CO adsorbed on Ru(130)/PtME ($E_S$ is indicated in the figure, $E_R = 1.00$ V), 0.1 mol $l^{-1}$ $H_2SO_4$ solution (CO saturated); (b) potential dependence of positive (filled square) and negative (open square) peaks of the $CO_L$ bipolar band on Ru(130)/PtME, and the variation of peak-to-peak intensity of the $CO_L$ bipolar band versus $E_S$.

time with electrode potential holding at 1.00 V after having collected the $R(E_S)$. The $R(E_S)$ and the time-resolved single-beam spectra $R(E_R)$ were then used to calculate the resultant spectra of time-resolution at $E_R$. We found that all resultant spectra of time resolution at $E_R$ were in fact identical, confirming that the bipolar IR feature comes uniquely from IR absorption of $CO_L$ at $E_S$. The bipolar IR feature of the $CO_L$ band is in fact a Fano-like line shape, which has been observed in transmission IR spectra of CO adsorbed on ultrathin Fe film (a few nanometers in film thickness) supported on Mg(0 0 1) under ultra-high-vacuum conditions [37–39]. Fano-like line shape has also been observed in ATR spectra of CO adsorbed on ultrathin film of Pt (7 nm in film thickness) [13] substrated on silicon under electrochemical conditions. Such Fano-like asymmetric spectrum was ascribed by Pucci and co-workers to the Fano effects [40], and interpreted as the non-adiabatic interaction of adsorbate vibrations with electronic excitations [39].

Apart from the bipolar IR feature, IR absorption of $CO_{ad}$ is obviously enhanced in considering that the appearance of the $CO_B$ band and the large value of peak-to-peak intensity ($I_{P-P}$). The results of Fig. 6a demonstrated that the Ru(130)/PtME electrode presents particular IR properties, which are different from those

of the Ru(370)/PtME mainly in the positive-going direction line shape of the $CO_L$ band.

The variations of the $I_{P-P}$ and the center of positive and negative peaks of the $CO_L$ bipolar band are plotted against $E_S$ in Fig. 6b. It can be seen that the $I_{P-P}$ maintains almost constant when $E_S$ is bellow 0.25 V, and it decreases quickly for $E_S$ varying from 0.25 to 0.50 V. It is evident that the decrease of $I_{P-P}$ is due to $CO_{ad}$ oxidation, as the intensity of the $CO_B$ band is decreased accordingly. The variation of the $I_{P-P}$ with $E_S$ indicates again that the onset oxidation potential of CO species adsorbed on Ru($n$)/PtME electrode is about 0.25 V, confirming the high electrocatalytic activity of Ru($n$)/PtME for CO oxidation. It is similar to Fig. 5c that, when $E_S$ is above 0.25 V, the center of both positive and negative peaks of the $CO_L$ bipolar band is deviated from the straight line that lasts for $E_S$ varying from 0.00 to 0.25 V. The Stark tuning rates of positive and negative peaks of the $CO_L$ bipolar band were measured, from the slope of the corresponding straight line in Fig. 5b, to be 55.9 and 56.6 $cm^{-1}\ V^{-1}$, respectively. These values are much smaller than the Stark tuning rate of the $CO_L$ band measured on Ru(370)/PtME electrode, in association with a decrease in Ru film thickness.

### 3.3.3. Effects of Ru film nanostructure on IR features of CO adsorbed on Ru(n)/PtME on the array

In situ MFTIR spectra of CO adsorbed on the individually addressable array for $E_S = 0.00$ V and $E_R = 1.00$ V are shown in Fig. 7. It can be seen that on all $ME_{ij}$ of the array, the broad $CO_B$ band situated between 1750 and 1850 $cm^{-1}$ maintains the positive-going direction, i.e., the direction of anti-absorption, while the intensity of the $CO_B$ band is varied on the array. However, the IR feature of the $CO_L$ band is changed progressively on Ru($n$)/PtME of the array as $n$ is increasing. The effects of Ru film nanostructure may be described in the following aspects:

1) The line shape of the $CO_L$ band is transformed from initial bipolar to positive-going monopolar. The bipolar IR feature of the $CO_L$ band can be observed from spectra recorded on $ME_{11}$ to $ME_{21}$, i.e., $n$ is increased from 50 to 170. Along with the increase of $n$, the intensity of the negative peak of the bipolar $CO_L$ band is decreased gradually, while that of the positive peak is augmented. Finally, the $CO_L$ band becomes a positive-going monopolar band on $ME_{22}$ to $ME_{33}$ on the array. It is evident that such a transform in line shape of the $CO_L$ band, i.e., from Fano-like asymmetric band to IR anti-absorption band, is caused by the consecutive variation of nanostructure of Ru film on the array. Pucci-Lehmann and coworkers [37] have demonstrated that the enhanced Fano-like asymmetric line shape of CO adsorbed on an ultrathin Fe film can be observed in transmission IR spectra, when Fe film thickness is smaller than 10 nm. However, when the Fe film thickness is increased above 10 nm, the reflection IR spectra of adsorbed CO yields normal symmetric line shape without enhancement. It is worthwhile to note that the Ru film thickness is much larger in the present study to yield the Fano-like line shape. As listed in Table 3, the Ru film thickness $\bar{l}$ and the Ru island size $\bar{d}$ on $ME_{11}$ to $ME_{21}$ ranges, respectively, from 66.3 to 84.6 nm and from 79.7 to 169.2 nm. However, further increase in $\bar{l}$ and $\bar{d}$ leads to the anti-absorption line shape.

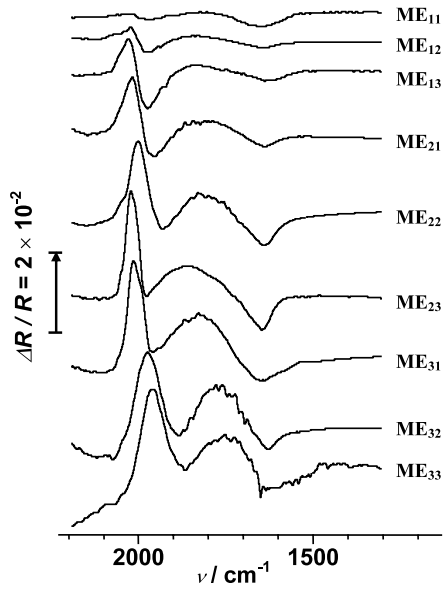


Fig. 7. Comparison of in situ FTIR spectra of CO adsorbed on $ME_{ij}$ on the array, $E_R = 1.00$ V, $E_S = 0.00$ V, 0.1 M $H_2SO_4$ solution saturated of CO.

2) The intensity of $CO_{ad}$ ($CO_L$ and $CO_B$) bands is increased gradually from $ME_{11}$ to $ME_{33}$, i.e., the IR absorption of CO adsorbed on nanostructured Ru film is significantly enhanced. It may be convenient to define an enhancement factor to systematically study this IR property. Since the $CO_B$ band is too broad to measure precisely the intensity, we take solely the $CO_L$ band of monopolar feature, i.e., the $CO_L$ band in spectra recorded on $ME_{22}$ to $ME_{33}$. The quantitative parameter of enhancement factor ($\Delta_{IR}$) is calculated using the following equation:

$$\Delta_{IR} = \frac{A^n_{CO_L}}{A^{n=0}_{CO_L}} \frac{1}{R_r} \quad (5)$$

where $A^{n=0}_{CO_L}$ signifies the integrated intensity of $CO_L$ band measured in the spectrum of substrate PtME electrode, i.e., the spectrum b in Fig. 5. $A^n_{CO_L}$ is the integrated intensity of the $CO_L$ band measured in spectra of $ME_{22}$ to $ME_{33}$. The surface relative roughness ($R_r$) measured in cyclic voltammetric studies is introduced in Eq. (5) to calibrate the

difference of real surface area of $ME_{ij}$ on the array. Since all $ME_{ij}$ possesses the same geometric area as that of the substrate PtME ($3.14 \times 10^{-4}$ $cm^2$), the real surface area of Ru($n$)/PtME is varied with $n$ and the quantity of CO adsorbed on Ru($n$)/PtME should be in direct proportion to $R_r$. The enhancement factor $\Delta_{IR}$ has been measured on $ME_{22}$ to $ME_{33}$ to be 15.5, 11.8, 12.7, 12.1 and 12.5, respectively.

3) The center of the $CO_L$ band is shifted when $n$ is increasing. The shift can be classed in two groups: for the Fano-like asymmetric spectra recorded on $ME_{11}$ to $ME_{13}$, the positive peak of the bipolar $CO_L$ band is blue-shifted from 2023 to 2028 $cm^{-1}$ and the negative peak of the bipolar $CO_L$ band is also blue-shifted from 1972 to 1977 $cm^{-1}$; for the anti-absorption $CO_L$ band in spectra recorded on $ME_{23}$ to $ME_{33}$, the $\nu_{CO_L}$ is red-shifted from 2024 to 1960 $cm^{-1}$. Nevertheless, the centers of $CO_{ad}$ bands in spectra recorded on $ME_{21}$ and $ME_{22}$ could not be included in above variation trends. It can also observe that the $CO_B$ band center manifests similar variation. It is obvious that $\nu_{CO_L}$ depends on the nanostructure of Ru film at a given electrode potential. If we take the Stark tuning rate 93 $cm^{-1}$ $V^{-1}$ measured on the Ru(370)/PtME to discuss the variation of $\nu_{CO_L}$, the shift of 64 $cm^{-1}$ from $ME_{22}$ to $ME_{33}$ may represent a shift in electrode potential of 688 mV. Since $E_S$ was set at 0.00 V to collect all single-beam spectra $R(E_S)$ in Fig. 7, the red-shift of $\nu_{CO_L}$ on Ru(370)/PtME could not be due to a shift in electrode potential. Such red-shift may imply that the nanostructure of Ru(370)/PtME can facilitate the d–π* back-donation between electrode surface and CO adsorbates, which leads to consequently the decrease of C–O stretching frequency.

4) The FWHM of anti-absorption $CO_L$ band is increased rapidly in the sequence from $ME_{22}$ to $ME_{33}$. The value of FWHM is measured on $ME_{22}$ to $ME_{33}$ to be 42, 43, 51, 81, 90 $cm^{-1}$, respectively. The increase in FWHM may be attributed to an inhomogeneous broadening. As illustrated by CV and STM studies, following $n$ increasing, the Ru islands in the film become larger and larger, and the surface of Ru film becomes more and more rough. The increase in $\bar{d}$ and $R_r$ implies that the number of different adsorption sites has been augmented. As a consequence, both linear- and bridge-bonded CO adsorbed on Ru($n$)/PtME with large $n$ give rise to the result of band broadening.

5) The relative level of spectral background at lower and higher wavenumber sides of the $CO_{ad}$ bands exhibits also regular changes. The level of spectral background at low wavenumber side of $CO_{ad}$ bands is lower than that at the high wavenumber side of the $CO_{ad}$ bands in spectra recorded on $ME_{11}$ to $ME_{21}$, and becomes higher than the level of spectral background at high wavenumber side of the $CO_{ad}$ band on $ME_{22}$ to $ME_{33}$. This result may indicate that, along with the variation of nanostructure of Ru film substrated on PtME over the array, the optical property of Ru film has been changed consecutively.

## 4. Conclusions

In this paper, surface combinatorial studies of IR properties of nanostructured Ru film were carried out by combining an individually addressable array and in situ microscope FTIR reflection spectroscopy. The Ru film of different nanostructure was prepared through electrodeposition on Pt microelectrode on the array. STM investigations illustrated that the Ru film was composed of island crystallites of nanometer size. The thickness of the Ru film and the size of Ru island crystallites, which were controlled in electrodeposition through varying the number of cycles ($n$) of potential scan, are increased consecutively from $ME_{11}$ to $ME_{33}$ on the array. The adsorption of CO was employed as probe molecule reaction, and in situ MFTIR spectral library of CO adsorbed on different nanostructures of Ru film and at different electrode potentials was acquired rapidly through surface combinatorial studies. It has revealed that the IR properties of CO adsorbed on Ru($n$)/PtME were varied regularly with nanostructure of Ru film. Along with the increase of $n$, the IR absorption of linear-bonded CO ($CO_L$) gives rise to an enhanced band that is transformed gradually from bipolar band to anti-absorption monopolar band. Such variation in IR features implies a change from Fano-like asymmetric spectral characteristics to abnormal IR features. Three other particular IR properties of nanostructured Ru film were also observed, which consist of (1) the large increase in the bandwidth, the maximum FWHM of the $CO_L$ band was measured on $ME_{33}$ of the array to be 90 $cm^{-1}$ that is about 37 $cm^{-1}$ larger than the FWHM value (53 $cm^{-1}$) of $CO_L$ band on nanometer thin Ru film electrodeposited on GC; (2) the large increase in Stark tuning rate, the highest value was measured on the $ME_{33}$ of the array to be 93 $cm^{-1}$ $V^{-1}$ that is much larger than the value (34 $cm^{-1}$ $V^{-1}$) measured on nanometer thin Ru film (86 nm of film thickness) electrodeposited on GC, and also larger than 52 $cm^{-1}$ $V^{-1}$ measured on a bulk Ru for $E_S$ varying in similar potential range; (3) the enhancement of IR absorption, an enhancement factor is varied between 11.8 and 15.5, and the maximum value of 15.5 has been determined on $E_{22}$ of the array. The results of in situ MFTIRS revealed that the onset oxidation potential of CO adsorbed on Ru($n$)/PtME electrode is about 0.25 V, which is about

110 mV lower than the onset oxidation potential of CO adsorbed on a bulk Ru electrode or on nanometer thin Ru film electrodeposited on GC. Such a high electrocatalytic activity of Ru($n$)/PtME is attributed to the synergy effect of interaction between Ru thin film and Pt substrate. This study demonstrated also that the thin film of Ru electrodeposited onto substrate of Pt microelectrode on the array under cyclic voltammetric conditions is a nanostructured material, which possesses particular IR properties and high electrocatalytic activity. The new surface combinatorial method and results described in this paper are of importance in understanding the fundamental of particular IR properties of nanostructured film material.

## Acknowledgements

This study was supported by grants from National Natural Science Foundation of China (90206039, 20021002) and State Education Ministry of China (01101), and by National Key Basic Research and Development Program (2002CB211804).

## References

[1] T. Ioroi, K. Yasuda, Z. Siroma, N. Fujiwara, Y. Miyazaki, J. Power Source 112 (2002) 583.
[2] A.V. Tripkovic, K.D. Popovic, B.N. Grgur, B. Blizanac, P.N. Ross, N.M. Markovic, Electrochim. Acta 47 (2002) 3707.
[3] Z. Jusys, R.J. Behm, J. Phys. Chem. B 105 (2001) 10874.
[4] W. Chen, Y.X. Jiang, S.G. Sun, Chin. Sci. Bull. 48 (2) (2003) 135.
[5] G.Q. Lu, S.G. Sun, S.P. Chen, L.R. Cai, J. Electroanal. Chem. 421 (1997) 19.
[6] G.Q. Lu, S.G. Sun, L.R. Cai, S.P. Chen, Z.W. Tian, K.K. Shiu, Langmuir 16 (2000) 778.
[7] M.S. Zheng, S.G. Sun, J. Electroanal. Chem. 500 (2001) 223.
[8] M.S. Zhen, S.G. Sun, S.P. Chen, J. Appl. Electrochem. 31 (2001) 749.
[9] W.G. Lin, S.G. Sun, J. Phys. Chem. B 106 (2002) 11778.
[10] P.A. Christensen, A. Hamnett, J. Munk, G.L. Troughton, J. Electroanal. Chem. 370 (1994) 251.
[11] R. Ortiz, A. Cuesta, O.P. Marquez, J. Marquez, J.A. Mendez, C. Gutierrez, J. Electroanal. Chem. 465 (1999) 234.
[12] G. Orozco, C. Gutierrez, J. Electroanal. Chem. 484 (2000) 64.
[13] Y. Zhu, H. Uchida, M. Watanabe, Langmuir 15 (1999) 8757.
[14] A.E. Bjerke, P. Griffiths, Anal. Chem. 71 (1999) 1967.
[15] R. Emory, W.E. Haskins, S. Nie, J. Am. Chem. Soc. 120 (1998) 8009.
[16] A. Hartstein, J.R. Kirtley, J.C. Tsang, Phys. Rev. Lett. 45 (1980) 201.
[17] M. Osawa, in: J.M. Chalmers, P.R. Griffiths (Eds.), Handbook of Vibrational Spectroscopy, Wiley, Chichester, 2002 (Chapter 1).
[18] T.A. Lestowa, M. Leyva-Lucero, E.R. Mendez, Opt. Commun. 183 (2000) 529.
[19] S. Baldelli, A.S. Epple, E. Anderson, J. Chem. Phys. 113 (2000) 5432.
[20] M.C. Pirrung, Chem. Rev. 97 (1997) 473–488.
[21] T.A. Dickison, D.R. Walt, Anal. Chem. 69 (1997) 3413.
[22] E. Danielson, M. Devenney, D.M. Giaquinta, J.H. Golden, R.C. Haushalter, E.W. McFarland, D.M. Poojary, C.M. Reaves, W.H. Weinberg, X.D. Wu, Science 279 (1998) 837.
[23] R.B. Van Dover, L.F. Schneemeyer, R.M. Fleming, Nature 392 (1998) 162.
[24] X.D. Xiang, X. Sun, G. Briceno, Y. Lou, K.A. Wang, H. Chang, W.G. Wallace-Freedman, S.W. Chen, P.G. Schultz, Science 288 (1995) 1738.
[25] S. Senkan, Angew. Chem. Int. Ed. 40 (2001) 312.
[26] E. Reddington, A. Sapienza, B. Gurau, R. Viswanathan, S. Sarangapani, E.S. Smotkin, T.E. Mallouk, Science 280 (1998) 1735.
[27] S.G. Sun, S.J. Hong, S.P. Chen, G.Q. Lu, H.P. Dai, X.Y. Xiao, Sci. China B 42 (1999) 261.
[28] H. Gong, S.P. Chen, Z.Y. Zhou, S.G. Sun, Chin. Sci. Bull. 46 (2001) 1612.
[29] W.F. Lin, M.S. Zei, M. Eiswirth, G. Erh, T. Iwasita, W. Vielstich, J. Phys. Chem. 103 (1999) 6968.
[30] W.F. Lin, T. Iwasita, W. Vielstich, J. Phys. Chem. B 103 (1999) 3250.
[31] C. Gutirrez, J.A. Caram, B. Beden, J. Electroanal. Chem. 305 (1991) 1289.
[32] R.C. Walker, M. Bailes, L.M. Peter, Electrochim. Acta 44 (1998) 289.
[33] K. Ataka, M. Osawa, Langmuir 14 (1998) 951.
[34] S.G. Sun, in: A. Wieckowski, E.R. Savinova, C.G. Vayenas (Eds.), Catalysis and Electrocatalysis at Nanoparticles Surfaces, Marcel Dekker, New York, 2003 (Chapter 21).
[35] A. Kabbabi, R. Faure, R. Durand, B. Beden, F. Hahn, J.M. Leger, C. Lamy, J. Electroanal. Chem. 444 (1998) 41.
[36] H.A. Gasteiger, N. Markovic, P.N. Ross, Jr., E. Cairns, J. Phys. Chem. 98 (1994) 617.
[37] A. Priebe, G. Fahsold, A. Pucci-Lehmann, J. Mol. Struct. 482–483 (1999) 237.
[38] O. Krauth, G. Fahsold, N. Magg, A. Pucci, J. Chem. Phys. 113 (2000) 6330.
[39] A. Priebe, G. Fahsold, A. Pucci, Surf. Sci. 482–485 (2001) 90.
[40] U. Fano, Phys. Rev. 124 (1961) 1866.